F 1/20296

# Emission of Sound From Turbulence Convected by a Parallel Mean Flow in the Presence of a Confining Duct

M. E. Goldstein

National Aeronautics and Space Administration

Glenn Research Center, Cleveland, Ohio 44135

and

S. J. Leib

Ohio Aerospace Institute

22800 Cedar Point Road, Brook Park, Ohio 44142

Emission of Sound from a Confining Duct
34 pages, 6 Figures

**Abstract**

An approximate method for calculating the noise generated by a turbulent flow within a semi-infinite duct of arbitrary cross section is developed. It is based on a previously derived high-frequency solution to Lilley's equation, which describes the sound propagation in a transversely-sheared mean flow. The source term is simplified by assuming the turbulence to be axisymmetric about the mean flow direction. Numerical results are presented for the special case of a ring source in a circular duct with an axisymmetric mean flow. They show that the internally generated noise is suppressed at sufficiently large upstream angles in a hard walled duct, and that acoustic liners can significantly reduce the sound radiated in both the upstream and downstream regions, depending upon the source location and Mach number of the flow.

# 1 Introduction

Considerable effort has been invested in developing a new generation of supersonic transports. One of the primary requirements was that the aircraft be quiet enough to meet or even exceed existing noise regulations, and it was

decided that a mixer-ejector nozzle concept would be used to help accomplish this objective. The idea was that a significant amount of the mixing noise would be generated internally within the nozzle, and could therefore be considerably reduced by using suitable acoustic liner designs. Data from recent tests using a prototype mixer-ejector show that the peak internal turbulence level is more than twice the external level. It is therefore important to develop prediction methods for this internally generated noise. A general theory based on Lighthill's equation was developed by Goldstein and Rosenbaum [1]. Dill, Oyediran and Krejsa [2] extended this analysis to account for mean-flow refraction effects. However, both theories involve the solution of a complicated Weiner-Hopf problem, which can only be explicitly worked out for a slug ( or 'top hat') mean velocity profile.

The experimental data suggest that the internal noise is of much higher frequency than the externally generated noise, in addition to being much more sensitive to nozzle geometry. Moreover, many of the most successful noise prediction schemes ( e.g. the MGB code) are based on high-frequency Lilley's-equation solutions. The present study is therefore directed toward developing a high-frequency Lilley's-equation solution that can be used to predict the internally generated noise. We suppose that the sound is gener-

ated by a superposition of statistically independent and acoustically compact, convecting-point quadruples and derive a formula for the high-frequency acoustic radiation generated by such sources when they are located within a semi-infinite, parallel-walled nozzle. In fact, we suppose that the mean flow is completely parallel, but allow the cross-sectional shape and velocity profile to be arbitrary (as shown in Figure 1a), in order to account for nozzle-geometry effects. The only variation in the streamwise direction is due to the boundary condition change at the nozzle exit, which is allowed to have an arbitrary shape. Finally, an arbitrary (frequency dependent) acoustic impedance boundary condition is imposed at the nozzle walls, in order to model an acoustically treated surface. The resulting solutions can then be superimposed to calculate the sound generated by an actual turbulent flow within a nozzle. The analysis can be used to guide the design of acoustic liners that may be required to absorb the noise radiated in specific directions or to design nozzle exit shapes that reduce the noise radiation below the flight path.

Goldstein [3] developed a formula (equation (5.9) of that reference) for the high-frequency sound radiation from a convecting-point quadruple source in an arbitrary, transversely sheared mean flow. This result was later extended

by Durbin [4] to account for a general (not necessarily parallel) mean flow. These formulas involve a ray-spreading factor that multiplies the product of a source function–which describes the actual acoustic sources-with some Doppler factors that account for the local source and mean flow convection effects. The spreading factor accounts for the mean-flow variation along the path of the radiated sound and can be calculated from geometric acoustics or ray tracing.

The present paper shows that Goldstein's [3] formula still applies to the internally-generated noise and that only the ray-tracing analysis which is used to calculate the ray-spreading factor needs to be modified in order to account for the effect of the nozzle walls. This is demonstrated in Section 2, where the notation is introduced and the Goldstein [3] and Durbin [4] analyses are reviewed in some detail.

Three-dimensional ray tracing is fairly complex and somewhat difficult to implement numerically, but it was shown in Ref. [3] that the three-dimensional ray-tracing calculation could be reduced to a much simpler two-dimensional one for the doubly-infinite jet flow considered in that paper. The rays can then be found by solving a single second-order equation. In section 3 we show that this can also be done in the present problem. The results

are applied to an actual turbulent flow in Section 4 and specialized to an axisymmetric mean flow in a round duct with circular exit plane in Section 5, where some numerical results are also presented. Some conclusions and recommendations for further work are given in Section 6.

# 2 Extension of Doubly Infinite Jet Solution to Account for Finite Nozzle Geometry

For definiteness, we consider a unidirectional, transversely-sheared, parallel mean flow

$$\mathbf{v} = \hat{\mathbf{i}} U(\mathbf{x}_t), \quad \rho = \bar{\rho}(\mathbf{x}_t), \quad c = \bar{c}(\mathbf{x}_t), \quad p = \text{constant}, \tag{1}$$

with velocity $\mathbf{v}$, density $\rho$, speed of sound $c$, and pressure $p$, exiting from a parallel-walled nozzle, as shown in Figure 1-a. The result which we obtain, however, is much more general and applies to more complicated flow configurations such as the one shown in Figure 1-b. Equation (1) is an exact solution of the inviscid, non-heat-conducting equations of motion for these configurations. $\mathbf{x} = \{x_1, x_2, x_3\}$ denote Cartesian coordinates with $x_1$ aligned with the direction of the mean flow, $\hat{\mathbf{i}}$ denotes the unit vector in this direction, and $\mathbf{x}_t = \{x_2, x_3\}$ denotes the transverse coordinate vector. The nozzle exit is

described by an arbitrary, three-dimensional curve C, as shown in the figure. The mean velocity $U$ is assumed to go smoothly to zero at the generators of the nozzle wall and to remain zero beyond that surface. The analysis does not therefore account for forward flight effects, but can easily be extended to do so.

Assuming that the ideal gas law applies, the linearized equation governing the acoustic propagation on this flow is [6]

$$\mathcal{L}p \equiv \frac{D}{Dt}\left(\frac{D^2p}{Dt^2} - \nabla\cdot\bar{c}^2\nabla p\right) + 2\bar{c}^2\nabla U\cdot\nabla\frac{\partial p}{\partial x_1} = \Gamma, \tag{2}$$

where $p$ now denotes the acoustic pressure fluctuation normalized by $\bar{\rho}\bar{c}^2$,

$$\frac{D}{Dt} \equiv \frac{\partial}{\partial t} + U\frac{\partial}{\partial x_1}, \tag{3}$$

denotes the convective derivative, and $t$ denotes the time. $\Gamma$ represents the acoustic source distribution and is given by

$$\Gamma = \frac{D}{Dt}\nabla\cdot\mathbf{f} - 2\nabla U\cdot\frac{\partial \mathbf{f}}{\partial x_1}, \tag{4}$$

when this quantity is produced by a fluctuating force $f_i$ per unit volume. In the absence of temperature fluctuations, Lilley's equation is obtained by replacing $f_i$ by the quadruple source distribution $f_i = \frac{\partial u_i u_j}{\partial x_j}$, where $u_i$ denotes the velocity fluctuation within the flow.

Since the problem is linear, and the second term in (4) is negligible compared to the first in the high-frequency limit, the solution for an arbitrary force distribution $f_i$ can be obtained by superposition of solutions, say $p_G$, to

$$\mathcal{L}\left(p_G \mathrm{e}^{-\mathrm{i}\omega t}\right) = \frac{D}{Dt}\delta\left(\mathbf{x}-\mathbf{x}^s\right)\mathrm{e}^{-\mathrm{i}\omega t}, \tag{5}$$

where $\omega$ is the frequency, $\mathbf{x}^s$ denotes the source position, and $\delta$ is the Dirac delta function.

## 2.1 Review of Durbin's high-frequency solution

By using matched asymptotic expansions, Durbin [4] showed that the solution to this problem is given by

$$p_G = p_G(\mathbf{x}|\mathbf{x}^s,\omega) = (1-Ms_1)\,\Phi \mathrm{e}^{ikS}, \tag{6}$$

in the high-frequency limit

$$k \equiv \omega/\bar{c}_\infty \to \infty, \tag{7}$$

where $\bar{c}_\infty$ is the speed of sound in the region of zero mean flow,

$$M \equiv U/\bar{c}_\infty, \tag{8}$$

S denotes the Eikenal, which satisfies the Eikenal equation

$$(1 - Ms_1)^2 - \left(\frac{\bar{c}}{\bar{c}_\infty}\right)^2 |\mathbf{s}|^2 = 0, \tag{9}$$

and

$$\mathbf{s} = \{s_1, s_2, s_3\} \equiv \nabla S. \tag{10}$$

The solution to this first-order partial differential equation can be obtained by the method of characteristics by calculating $S$ along the rays $\mathbf{x}(\tau)$ , which are determined by the ordinary differential equations

$$\dot{s}_1 = 0, \tag{11}$$

$$\dot{x}_1 = s_1 \left[1 - \left(\frac{U}{\bar{c}}\right)^2\right] + \frac{U\bar{c}_\infty}{\bar{c}^2}, \tag{12}$$

$$\left.\begin{aligned} \dot{x}_i &= s_i \\ \dot{s}_i &= \tfrac{1}{2}\tfrac{\partial}{\partial x_i}\left(\tfrac{s_1 U - \bar{c}_\infty}{\bar{c}}\right)^2 \end{aligned}\right\}, \quad i = 2, 3, \tag{13}$$

subject to the initial conditions at the source position $\mathbf{x}^s$ that the initial ray velocity is proportional to the initial ray direction, say $\{\cos\mu, \sin\mu\cos\lambda, \sin\mu\sin\lambda\}$, i.e. that

$$\dot{\mathbf{x}}_s = \gamma_s\{\cos\mu, \sin\mu\cos\lambda, \sin\mu\sin\lambda\}, \tag{14}$$

where the dot denotes differentiation with respect to $\tau$, the subscript $s$ denotes quantities evaluated at the source position $\mathbf{x}^s$, and the proportionality

constant $\gamma_s$ is given by

$$\gamma_s{}^{-2} = (\bar{c}_s/\bar{c}_\infty)^2 \left[1 - \left(\frac{U_s}{\bar{c}_s}\sin\mu\right)^2\right]. \tag{15}$$

As pointed out by Durbin [4], Eq. (15) without the subscript $s$, and with $\mu$ replace by the polar angle $\theta$, relates the ray speed to the ray direction at all points along a ray.

The amplitude function $\Phi$ is given by

$$\Phi \equiv \frac{1}{4\pi\bar{c}\bar{c}_\infty(1 - M_s s_1)}\sqrt{\frac{\bar{\rho}\gamma_s^3 \sin\mu}{\bar{\rho}_s \gamma J}}, \tag{16}$$

where $J$ denotes the Jacobian determinant

$$J = \left|\frac{\partial(x_1, x_2, x_3)}{\partial(\sigma, \mu, \lambda)}\right|, \tag{17}$$

with $d\sigma = |d\mathbf{x}|$ denoting the distance along the ray.

Once these equations are solved, the Eikenal can be found by integrating the equation

$$\dot{S} = \mathbf{s} \cdot \dot{\mathbf{x}}, \tag{18}$$

and the velocity fluctuation $\mathbf{u}_G$, corresponding to the acoustic pressure perturbation $p_G$, can be calculated from

$$\mathbf{u}_G = \bar{c}^2 \mathbf{s} \Phi \mathrm{e}^{\mathrm{i}kS}/\bar{c}_\infty. \tag{19}$$

The important thing to notice is that the derivation of these results is completely independent of any boundary conditions that are imposed on the surface $\Sigma$ of the duct, and the termination curve C of the duct exit. The latter gives rise to the so-called defracted radiation which (Pierce [7]) is of higher order in frequency than the direct and reflected radiation and can therefore legitimately be neglected in the high-frequency limit-though it can certainly be important in the upstream direction.

## 2.2 Modification of solution to account for the duct walls

The conditions at the surface of the duct are accounted for by imposing boundary conditions on the solutions to the ray equations (11) to (13) at the point where the rays reach the boundary to produce a reflected wave, say $\{p_+, u_+\}$, corresponding to the incident wave, say $\{p_-, u_-\}$. (See, for example, [7].)

The reflected wave is still given by equations (6) with (16), but multiplied by a constant reflection coefficient, say $\mathcal{R}$. The Eikenal S is obtained by integrating (18) through the reflection.

Thus, the pressure and velocity on the boundary $\Sigma$ are given by

$$p_G = \Phi\,(1 + \mathcal{R})\,\mathrm{e}^{\mathrm{i}kS}, \tag{20}$$

and

$$\mathbf{u}_G = \frac{\bar{c}^2\Phi}{\bar{c}_\infty}\,(\mathbf{s}_- + \mathcal{R}\mathbf{s}_+)\,\mathrm{e}^{\mathrm{i}kS} \tag{21}$$

(recall that $U$ is assumed to be zero at $\Sigma$).

The usual impedance boundary condition for a locally-reacting surface involves only the normal component of the velocity $\mathbf{u}_G$, and therefore only the normal component of the propagation vector $\mathbf{s}$. This condition is usually expressed in terms of an impedance, say $Z$ (which can, in general, be a function of the frequency $\omega_s$), as

$$Z = \bar{\rho}\bar{c}^2\frac{p_G}{\mathbf{u}_G \cdot \hat{\mathbf{n}}} \quad \text{for } \mathbf{x} \text{ on } \Sigma, \tag{22}$$

where $\hat{\mathbf{n}}$ denotes the unit normal to $\Sigma$. Moreover, the normal component of $\mathbf{s}$ changes sign, i.e.

$$\mathbf{s}_- \cdot \hat{\mathbf{n}} = -\mathbf{s}_+ \cdot \hat{\mathbf{n}} \quad \text{for } \mathbf{x} \text{ on } \Sigma. \tag{23}$$

Substituting this along with (21) into (22) yields the following expression for the reflection coefficient

$$\mathcal{R} = \frac{\eta + 1}{\eta - 1}, \tag{24}$$

where

$$\eta \equiv -(\mathbf{s}_- \cdot \hat{\mathbf{n}})\,\zeta, \tag{25}$$

where $\zeta = Z/\bar{\rho}_\infty \bar{c}_\infty$ is a normalized impedance. Notice that $Z \to \infty$ and $\mathcal{R} \to 1$ for a hard wall.

On the other hand, the tangential component of $\mathbf{s}$, namely $s_1$, remains unchanged by the reflection, and it therefore follows from (11) that

$$s_1 = \text{ constant}, \tag{26}$$

which is equal to the far-field value of this quantity for any ray that propagates to infinity (which are the only ones we are interested in here). In this region (where the mean flow is zero), the acoustic rays are straight lines and are therefore given by

$$\mathbf{x} = \mathbf{x}^s + R\,(\cos\theta_\infty, \sin\theta_\infty \cos\phi_\infty, \sin\theta_\infty \sin\phi_\infty)\,, \tag{27}$$

where $R$ can be taken as the distance between the source point and the observation point, and $\theta_\infty$ and $\phi_\infty$ denote the far-field polar and circumferential angles, respectively, shown in Figure 1.

It therefore follows from Eqs. (11) to (13) and the Eikenal equation (18) that $\dot{R} = 1$, and that

$$s_1 = \cos\theta_\infty. \tag{28}$$

The Jacobian determinant (17) becomes

$$J = R^2 \sin\theta_\infty \left| \frac{\partial(\theta_\infty, \phi_\infty)}{\partial(\mu, \lambda)} \right|, \tag{29}$$

and it now follows from (12), (14), and (28) that

$$\gamma_s \cos\mu = \left[ 1 - \left( \frac{U_s}{\bar{c}_s} \right)^2 \right] \cos\theta_\infty + \frac{U_s \bar{c}_\infty}{\bar{c}_s^2}. \tag{30}$$

Eliminating $\gamma_s$ between this and equation (15) shows that $\theta_\infty$ depends only on $\mu$, and not $\lambda$, and that

$$\gamma_s{}^3 \left( \frac{\bar{c}_s}{\bar{c}_\infty} \right)^2 = \frac{\sin\theta_\infty}{\sin\mu} \frac{d\theta_\infty}{d\mu}. \tag{31}$$

Inserting this into (16) and using (29) shows that

$$\Phi \to \frac{\bar{\mathcal{R}}}{4\pi R \bar{c}_\infty^2 (1 - M_s \cos\theta_\infty)} \sqrt{\left| \frac{d\lambda}{d\phi_\infty} \right|}, \tag{32}$$

where we have used the ideal gas law to obtain this result and put

$$\bar{\mathcal{R}} \equiv \prod_{i=1}^{m} \mathcal{R}_i, \tag{33}$$

where the $\mathcal{R}_i$ denote the individual reflection coefficients for each of the $m$ reflections that the ray undergoes before leaving the duct. Also, it follows from (13), (18) and (28) that

$$S = (x_1 - x_1{}^s) \cos\theta_\infty + S_0(\mathbf{x}_t | \mathbf{x}_t{}^s). \tag{34}$$

## 2.3 Application to moving point source

As indicated in the Introduction, the sound radiated by an actual turbulent flow can be calculated in terms of the pressure field $p$ generated by a superposition of point quadrupole sources moving downstream with the mean flow. We therefore consider the source distribution

$$\Gamma = \frac{D}{Dt}\frac{\partial^2}{\partial x_i \partial x_j} e^{-i\omega_s t}\delta\left(\mathbf{x} - \mathbf{x}_t{}^s - \hat{\imath}U_c t\right) Q_{ij}, \tag{35}$$

where $U_c$ denotes the convection speed of the source whose strength is $Q_{ij}$.

The corresponding acoustic field can be calculated from the fixed source solution $p_G$ by superposing Fourier components and using the Green's formula ([3])

$$p = \frac{Q_{ij}}{2\pi}\int\int_{-\infty}^{\infty}\int p_G(\mathbf{x}|\mathbf{y},\omega)e^{-i\omega(t-\tau)}\frac{\partial^2}{\partial x_i{}^s \partial x_j{}^s}e^{-i\omega_s\tau}\delta(\mathbf{y} - \mathbf{x}^s - \hat{\imath}U_c t)d\mathbf{y}d\tau d\omega. \tag{36}$$

Integrating by parts to transfer the derivatives from the source term to the Green's function, and carrying out the integrations with respect to $\mathbf{y}_t$ and $\tau$ gives

$$p = \frac{Q_{ij}}{2\pi U_c}e^{-i\omega_s t}\int_{-\infty}^{\infty}\int e^{i(\omega-\omega_s)(x_1{}^s/U_c - t)}\frac{\partial^2}{\partial x_i{}^s \partial x_j{}^s}p_G(\mathbf{x}|\mathbf{x}^s,\omega)dx_1{}^s d\omega. \tag{37}$$

For clarity, we begin with the case where only a single ray reaches the observer. The result will then be corrected for multiple ray effects in a

relatively obvious manner. Inserting equations (6), (28) and (34) into (37), and using the fact that (at lowest approximation) the partial derivatives operate only on the frequency-dependent terms in the exponent, we obtain

$$p = (1 - M\cos\theta_\infty)\, e^{-i\omega_s t}\frac{Q_{ij}}{2\pi U_c}\int\int \Phi e^{i(\omega-\omega_s)(x_1{}^s/U_c - t)} \times \frac{\partial^2}{\partial x_i{}^s \partial x_j{}^s} e^{\frac{i\omega}{\bar{c}_\infty}[(x_1 - x_1{}^s)\cos\theta_\infty + S_0]} dx_1{}^s d\omega. \tag{38}$$

Then, carrying out the integration, first with respect to $x_1{}^s$ (to obtain a $\delta$-function), and then with respect to $\omega$, shows that

$$p = \frac{-(1 - M\cos\theta_\infty)\,\sigma_i\sigma_j Q_{ij}}{(1 - M_c\cos\theta_\infty)} k_s{}^2 \Phi e^{\frac{i\omega_s}{\bar{c}_\infty(1 - M_c\cos\theta_\infty)}(x_1\cos\theta_\infty + S_0 - \bar{c}_\infty t)}, \tag{39}$$

where we have put $M_c = U_c/\bar{c}_\infty$, $k_s = \omega_s/\bar{c}_\infty$ and

$$\sigma_1 = \frac{\cos\theta_\infty}{1 - M_c\cos\theta_\infty} \quad ; \quad \sigma_i = \frac{-1}{1 - M_c\cos\theta_\infty}\frac{\partial S_0}{\partial x_i{}^s}, \text{ for } i = 2, 3. \tag{40}$$

Then it follows from equation (32) that

$$|p|^2 \to \frac{k_s{}^4 \left|Q_{ij}\sigma_i\sigma_j\right|^2 \left|\bar{\mathcal{R}}\right|^2}{(4\pi R)^2 \bar{c}_\infty^4 (1 - M_s\cos\theta_\infty)^2 (1 - M_c\cos\theta_\infty)^2} \left|\frac{d\lambda}{d\phi_\infty}\right|, \tag{41}$$

in the far field where $M = 0$, which, except for some minor notational changes, and the inclusion of the reflection coefficient $\bar{\mathcal{R}}$, is the same as equation (5.9) given in Ref. [3]. The normalized wall impedance, $\zeta$, which appears in this equation through the reflection coefficient, $\bar{\mathcal{R}}$ , must be eval-

uated at the actual (or observation) frequency

$$\omega = \omega_s / \left(1 - M_c \cos\theta_\infty\right), \tag{42}$$

and not the source frequency $\omega_s$.

It is convenient to allow the transverse orientation of the quadrupoles to vary with source position. This amounts to changing the orientation of the $\mathbf{x}^s$ coordinate system or, equivalently, referencing the angle $\lambda$ to a different angle, say $\lambda_0(\mathbf{x}^s)$. Then it follows from the results given in Ref. [3] that $\sigma_2$ and $\sigma_3$ are given explicitly by

$$\sigma_2 = \frac{-q_s \cos\left(\lambda - \lambda_0\right)}{1 - M_c \cos\theta_\infty} \quad ; \quad \sigma_3 = \frac{-q_s \sin\left(\lambda - \lambda_0\right)}{1 - M_c \cos\theta_\infty}, \tag{43}$$

where

$$q \equiv \sqrt{\frac{\left(1 - M\cos\theta_\infty\right)^2}{\left(\bar{c}/\bar{c}_\infty\right)^2} - \cos^2\theta_\infty}. \tag{44}$$

When multiple rays (which we individuate by a superscript in parentheses) reach the observer, the far-field pressure is given by the somewhat more complicated formula

$$|p|^2 \to \frac{{k_s}^4 Q_{ij} Q^\star_{kl} D_{ijkl}}{\left(4\pi R\right)^2 \bar{c}_\infty^4 \left(1 - M_s \cos\theta_\infty\right)^2 \left(1 - M_c \cos\theta_\infty\right)^2}, \tag{45}$$

where $\star$ denotes the complex conjugate, and the dependence on the transverse

source coordinates $r_s, \phi_s$, and the emission angle $\lambda$ enters through

$$D_{ijkl} \equiv \sum_{n,m=1}^{\kappa} \sigma_i^{(n)} \sigma_j^{(n)} \sigma_k^{(m)} \sigma_l^{(m)} \bar{\mathcal{R}}^{(n)} \bar{\mathcal{R}}^{(m)*} \sqrt{\left|\frac{\partial \lambda^{(n)}}{\partial \phi_\infty}\right| \left|\frac{\partial \lambda^{(m)}}{\partial \phi_\infty}\right|} e^{i\frac{\omega}{c_\infty}\left(S_0^{(n)} - S_0^{(m)}\right)}, \tag{46}$$

where $\kappa$ denotes the number of rays reaching the observer.

# 3 Reduction of Order of Ray Equations

Goldstein [3] introduced the two-dimensional ray distance $\mathcal{S}$ defined by (see equation (2.19) of that reference),

$$\left|\frac{d\mathbf{x}_t}{d\mathcal{S}}\right| = 1. \tag{47}$$

It follows from equations (14), (15) (generalized to arbitrary position along a ray), (44) and (28) that $\tau$ is related to $\mathcal{S}$ by

$$\frac{d\mathcal{S}}{d\tau} = q. \tag{48}$$

Equations (13) can then be combined to obtain the second-order system

$$\frac{d}{d\mathcal{S}} q \frac{d\mathbf{x}_t}{d\mathcal{S}} = \nabla_t q, \tag{49}$$

where $\nabla_t$ denotes the cross stream divergence. This is the same as equation (2.23) of ref. [3], where it is shown, by introducing the polar coordinates

$$\phi = \tan^{-1}(x_3/x_2), \quad r = \sqrt{{x_2}^2 + {x_3}^2}, \tag{50}$$

that it can be reduced to the single second-order equation

$$\frac{1}{I}\frac{d}{d\phi}\frac{r^2 q}{I} = \frac{\partial q}{\partial \phi}, \tag{51}$$

where

$$I \equiv \sqrt{r^2 + \left(\frac{dr}{d\phi}\right)^2}, \tag{52}$$

which is to be solved subject to the initial conditions

$$r = r_s \;\; ; \;\; \frac{dr}{d\phi} = r_s \cot(\lambda - \phi_s), \text{ at } \phi = \phi_s. \tag{53}$$

Inserting equations (13) and (48) into the boundary condition (23), using (50) and taking $\phi$ as the independent variable, shows that the appropriate boundary condition for equation (51) is

$$\frac{1}{I_+}\left[\frac{dr_+}{d\phi} - r + \tan(\phi - \beta)\right] = \frac{1}{I_-}\left[\frac{dr_-}{d\phi} - r - \tan(\phi - \beta)\right], \quad \text{for } \mathbf{x} \text{ on } \Sigma, \tag{54}$$

where we have put

$$\hat{\mathbf{n}} \equiv \{\cos\beta, \sin\beta\}. \tag{55}$$

This boundary condition must be imposed on all rays reaching the cylindrical surface containing the duct wall whenever

$$x_1 \leq x_e(x_2, x_3), \tag{56}$$

where $x_1 = x_e(x_2, x_3)$ is the equation for the termination curve $C$. $x_1$ can be calculated as a function of $\phi$ along the ray by inserting (28), (48), (50), and (52) into (13) to obtain

$$\frac{dx_1}{d\phi} = \frac{I}{q}\left(\frac{\bar{c}_\infty}{\bar{c}}\right)^2 \left\{\left[\left(\frac{\bar{c}}{\bar{c}_\infty}\right)^2 - M^2\right]\cos\theta_\infty + M\right\}. \tag{57}$$

# 4 Application to Sound Radiated by Actual Turbulent Flows

Equation (45) can be used to calculate the power spectral density of a spectral distribution of sources of band width $\Delta\omega_s$ by putting $Q_{ij}Q^*_{kl}$ equal to $\Psi_{ijkl}\Delta\omega_s$ . However, pressure spectra are measured per unit observation frequency $\Delta\omega$

$$\Delta\omega = \frac{\Delta\omega_s}{1 - M_c\cos\theta_\infty}, \tag{58}$$

(see Eq. (42)) and it therefore follows that the directivity of the spectra at constant source frequency $\omega_s$ (due to a source at $\mathbf{x}^s$) is given by

$$\frac{1}{\Delta\omega}|p|^2 \to \frac{k_s^{\,4}\Psi_{ijkl}D_{ijkl}}{(4\pi R)^2\,\bar{c}_\infty^4\,(1 - M_s\cos\theta_\infty)^2\,(1 - M_c\cos\theta_\infty)}\left|\frac{d\lambda}{d\phi_\infty}\right|. \tag{59}$$

This result can now be used to calculate the sound emitted by an actual turbulent flow by assuming that the turbulent eddies behave like compact

sound sources, and using Lilley's equation to show that the spectral source strength $\Psi_{ijkl}$ is related to the fourth-order, two-point, time-delayed correlation function of the turbulence

$$R_{ijkl}(\mathbf{x}^s, \boldsymbol{\xi}, \tau) = \overline{u_i' u_j' u_k'' u_l''} - \overline{u_i' u_j'}\ \overline{u_k'' u_l''}, \tag{60}$$

in the usual way by

$$\Psi_{ijkl} = \int\int \mathrm{e}^{-\mathrm{i}\omega_s \tau} R_{ijkl}(\mathbf{x}^s, \boldsymbol{\xi}, \tau) d\boldsymbol{\xi} d\tau, \tag{61}$$

where the single prime indicates that the quantity is evaluated at the position and time $(\mathbf{x}^{s\prime}, t)$, the double prime indicates the position and time $(\mathbf{x}^{s\prime\prime}, t+\tau)$,

$$\boldsymbol{\xi} = \mathbf{x}^{s\prime\prime} - \mathbf{x}^{s\prime} - \hat{\mathbf{i}} U_c \tau, \tag{62}$$

and

$$\mathbf{x}^s = \left\{ x_1^{s\prime}, \tfrac{1}{2}\left(x_2^{s\prime} + x_2^{s\prime\prime}\right), \tfrac{1}{2}\left(x_3^{s\prime} + x_3^{s\prime\prime}\right) \right\} \tag{63}$$

denotes the mean position of the source.

Since the sound field is always produced by a distribution of sources rather than by a single point source, the final result will involve an integral of Eq. (59) (and consequently of Eq. (46)) over the transverse source coordinates $r_s$ and $\phi_s$. Then, since $S_0^{(n)}$ is a function of these coordinates, the contribution

from the cross-coupling terms in (46) will be smaller than the contribution of the $m = n$ terms by a factor of (at least) $\omega^{-1/2}$, which in a strict asymptotic sense is negligible in the high-frequency limit. However, the zero-mean-flow computations of Boyd, Kempton and Morfey [8] suggest that the asymptotic convergence may be relatively slow for sources close to the wall (which result in small values of $S_0^{(n)} - S_0^{(m)}$ in Eqn. (46)), and that the interference effects may not be insignificant even at relatively high frequencies – particularly at small angles to the downstream axis where the sound field in expected to be maximal. However, the turbulent flows, which are of interest here, will probably introduce significant random fluctuations in the phases of the disturbances, which will tend to uncorrelate the pressure fluctuations corresponding to different ray paths. We therefore feel that it is best to neglect the interference effects, which amounts to replacing Eq. (46) with

$$D_{ijkl} = \sum_{n=1}^{\kappa} \sigma_i^{(n)} \sigma_j^{(n)} \sigma_k^{(n)} \sigma_l^{(n)} \left| \bar{\mathcal{R}}^{(n)} \right|^2 \left| \frac{\partial \lambda^{(n)}}{\partial \phi_\infty} \right|. \tag{64}$$

Since the fourth-order correlation tensor is very difficult to measure experimentally, or even calculate numerically, it is usual to assume that the turbulence is quasi-normal, and, consequently, that $R_{ijkl}$ can be expressed as

the product of second-order correlations ([9], [10])

$$R_{ijkl} = R_{ik}R_{jl} + R_{il}R_{jk}. \tag{65}$$

In order to simplify this further, Goldstein and Rosenbaum [11], Kerschen [12], and, more recently, Béchara *et al.* [13] and Khavaran [14] , assumed that the turbulence is axisymmetric about the direction of the mean flow. The analysis given in Ref. [1] (see also [2]) then shows that

$$\begin{aligned}\sigma_i\sigma_j\sigma_k\sigma_l\Psi_{ijkl} &= |\boldsymbol{\sigma}|^4 \int\int \mathrm{e}^{-\mathrm{i}\omega_s\tau}\bar{Q}_0 d\boldsymbol{\xi}d\tau - 2\left(\sigma_2\sigma_3\right)^2 \int\int \mathrm{e}^{-\mathrm{i}\omega_s\tau}\left(\bar{Q}_{23} - \bar{Q}_{22}\right) d\boldsymbol{\xi}d\tau \\ &+ \sigma_i^2\sigma_j^2 \int\int \mathrm{e}^{-\mathrm{i}\omega_s\tau}\bar{Q}_{ij} d\boldsymbol{\xi}d\tau,\end{aligned} \tag{66}$$

where we have dropped the superscript $(n)$ on the $\sigma_i$, and

$$\begin{aligned}\bar{Q}_{11} &= R_{11}^2 - R_{12}^2 \\ \bar{Q}_{12} = \bar{Q}_{13} &= R_{12}^2 + R_{11}R_{22} \\ \bar{Q}_{22} = \bar{Q}_{33} &= R_{22}^2 - R_{12}^2 \\ \bar{Q}_{23} &= R_{22}^2 - R_{23}^2 \\ \bar{Q}_0 &= R_{12}^2\end{aligned} \tag{67}$$

are symmetric in their indices.

# 5 Application to Round Duct with Axisymmetric Mean Flow

Goldstein [3] showed that Eqs. (51) - (53) can be solved analytically when the mean flow is axisymmetric. A similar procedure can be used to obtain an analytical solution to the present problem, but it is probably easier to solve it numerically. However, it is important to notice that, in this case, the resulting solution, whether obtained analytically or numerically, will depend on $\lambda$, $\phi$ and $\phi_s$ (where $\phi_s$ is the circumferential angle of the source point) only in the combinations $\phi - \phi_s$ and $\lambda - \phi_s$, since the coefficient q in Eq. (51) is independent of $\phi$, i.e., $\phi$ appears only as an independent variable. This, in particular, implies that $\lambda - \phi_s$ is a function of $\phi_\infty - \phi_s, r_s$ and $\theta_\infty$. Moreover, calculations of the ray trajectories for sources located within the nozzle show that $\lambda$ is a discontinuous, multi-valued function of $\phi_\infty$, due to the sudden change of boundary conditions at the nozzle lip. This is illustrated in figure 2, which is a plot of $\phi_\infty$ vs. $\lambda$ for the indicated source location. Thus, even though $\phi_\infty$ is necessarily a single-valued function of $\lambda$, the figure shows that the converse is certainly not true. It follows that

$$\sum_{n=1}^{\kappa} \int_0^{2\pi} \sin^p\left(\lambda^{(n)} - \phi_s\right) \cos^q\left(\lambda^{(n)} - \phi_s\right) \left|\bar{\mathcal{R}}^{(n)}\right|^2 \left|\frac{d\lambda^{(n)}}{d\phi_\infty}\right| d\phi_s$$

$$= \sum_{n=1}^{\kappa} \int_0^{2\pi} \sin^p\left(\lambda^{(n)} - \phi_s\right) \cos^q\left(\lambda^{(n)} - \phi_s\right) \left|\bar{\mathcal{R}}^{(n)}\right|^2 \left|\frac{d\left(\lambda^{(n)} - \phi_s\right)}{d\phi_s}\right| d\phi_s \quad (68)$$

$$= \int_0^{2\pi} \sin^p \bar{\lambda} \cos^q \bar{\lambda} \left|\bar{\mathcal{R}}^{(n)}\right|^2 d\bar{\lambda} \quad \text{for } p, q = 0, 1, 2,$$

since, for a given $r_s$ and $\theta_\infty$, $\bar{\mathcal{R}}$ depends on $\phi_\infty - \phi_s$ only through $\lambda - \phi_s$. The sum in Eq. (68) must be taken over all $\lambda^{(n)}$ values corresponding to any given value of $\phi_\infty$, in order to account for all of the rays reaching a given observation point.

If we now choose the reference angle $\lambda_0$ in Eq. (43) to be equal to $\phi_s$, the quadrupole sources will have the same orientation relative to the radial direction for all $\phi_s$, i.e. the quadrupole source distribution in Eq. (59) will be axisymmetric when $\Psi_{ijkl}$ is independent of $\phi_s$. Then, since equations (43), (44), (64), and (68) show that the entire $\phi_\infty$ dependence in (59) is of the form (68), it follows that the sound field $|p|$ emitted by a ring of uncorrelated, equi-strength quadrupole sources with radius $r_s$, and the same orientation relative to the radial direction, is independent of the circumferential observation angle $\phi_\infty$, i.e. it is axisymmetric.

When $\left|\bar{\mathcal{R}}\right| = 1$ (i.e. for a hard-walled duct), it follows from equations (43), (44), (66) and (68) that

$$\sum_{n=1}^{\kappa} \int_0^{2\pi} \sigma_i{}^{(n)} \sigma_j{}^{(n)} \sigma_k{}^{(n)} \sigma_l{}^{(n)} \Psi_{ijkl} \left|\bar{\mathcal{R}}^{(n)}\right|^2 \left|\frac{\partial \lambda^{(n)}}{\partial \phi_\infty}\right| d\phi_s =$$

$$\frac{2\pi}{(1-M_c\cos\theta_\infty)^4}\left[\frac{{q_s}^4}{8}\int\int \mathrm{e}^{-\mathrm{i}\omega_s\tau}\left(8\bar{Q}_0+7\bar{Q}_{22}+\bar{Q}_{23}\right)d\xi d\tau\right.$$
$$+2\cos^2\theta_\infty {q_s}^2\int\int \mathrm{e}^{-\mathrm{i}\omega_s\tau}\left(\bar{Q}_{12}+\bar{Q}_0\right)d\xi d\tau +$$
$$\left.+\cos^4\theta_\infty\int\int \mathrm{e}^{-\mathrm{i}\omega_s\tau}\left(\bar{Q}_{11}+\bar{Q}_0\right)d\xi d\tau\right]. \qquad (69)$$

For isotropic turbulence $\bar{Q}_{ij}=7\bar{Q}_0$, and it follows from Eqns. (43) and (44) that Eq. (69) is independent of $\theta_\infty$ when $M_s=M_c$. This means that the sound radiated by a ring source in a hard-walled duct is not only independent of the mean velocity profile within the jet, but is also unaffected by the presence of the duct when all rays reach the far field. Of course, this result only applies when the phase cancelation between multiple rays can be neglected. Also, since $r_s d\phi_s$ is the element of arc length, the total sound radiated by the ring source will be directly proportional to the radius $r_s$.

## 5.1 Numerical results

Results for the directivity patterns due to a ring source within a round duct were computed for a constant mean speed of sound, $\bar{c}\equiv\bar{c}_\infty$, and mean Mach number profiles of the form

$$M(r)=M_0\frac{\mathrm{e}^{-ar^b}-\mathrm{e}^{-a}}{1-\mathrm{e}^{-a}}, \qquad (70)$$

where $M_0$ is the centerline Mach number and the parameters $a$ and $b$ are used to control the profile shape.

The source terms in Eq. (66) were evaluated using the relations given by Khavaran [14] for axisymmetric turbulence. The anisotropy is characterized by the two parameters $\overline{u_2^2}/\overline{u_1^2}$ and $L_2/L_1$, where $\overline{u_1^2}$ and $\overline{u_2^2}$ are the streamwise and transverse mean square turbulent velocities, respectively, and $L_1$ and $L_2$ are the corresponding correlation lengths (see ref. [14]). Values for the anisotropy parameters of $\overline{u_2^2}/\overline{u_1^2} = 0.6$ and $L_2/L_1 = 0.5$ were used in the calculations.

Figure 3 shows the results for the far-field directivity

$$\mathcal{D} = \frac{2\,|p|^2}{\Delta\omega}\frac{(4\pi R)^2\,\bar{c}_\infty^4}{k_s^4\Psi_{1111}}, \tag{71}$$

vs. far-field polar angle, $\theta_\infty$, for a ring source at $r_s = 0.75r_0, x_1{}^s = -2.0r_0$, where $r_0$ is the duct radius, and a centerline Mach number of 1.5 with $a = 0.1, b = 6$, for a hard-walled duct and a soft-walled duct of various impedances.

For sufficiently small far-field polar angles outside the zone of silence, all rays emanating from the source reach the far field and, for the perfectly-reflecting, hard-walled duct considered here, the duct has no effect on the far-field sound. At far-field positions beginning in the upstream quadrant

( i.e. $\theta_\infty > \pi/2$ ), however, some of the rays become trapped within the duct, causing the sound pressure levels to be reduced at these angles. The hard-walled duct, therefore, only effects the sound field at sufficiently large angles to the downstream axis which, in fact, lie in the upstream quadrant as indicated in the figure. Since the number of rays reaching the far field rapidly decreases as $\theta_\infty \to \pi$, there is a sharp drop in the far-field sound.

However, the soft-walled duct starts to effect the sound field as soon as wall reflections begin. Since an increasing number of rays reflect (an increasing number of times) off the walls as the polar angle increases there is a substantial decrease in the far-field sound relative to the hard-wall case. The wall impedances $\zeta = (1, -1)$ and $\zeta = (2, -1)$ are seen to reduce the peak noise level by nearly 5 dB, relative to the hard wall case. The results suggest that the magnitude and phase of the normalized wall impedance can significantly effect the peak sound level, and a detailed parameter study to find the optimal value should be carried out.

Figures 4 and 5 show the effect of the source position on the far-field sound. The rays undergo fewer wall reflections when the source is closer to the nozzle exit (Fig. 4), and the acoustic liner therefore provides less noise suppression. When the source is closer to the duct centerline (Fig. 5), all

rays exit the duct without reflecting off the wall when the far-field polar angle is sufficiently small, and the acoustic liner has no effect on the sound field. Wall reflections start to occur when the polar angle is increased, and the liner reduces the far-field sound, but only by a relatively small amount - again due to fewer wall reflections.

Figure 6 illustrates the effect of centerline Mach number on the liner effectiveness. At the subsonic Mach number ($M(0) = 0.9$) for which this result was obtained, a wall impedance of $\zeta = (1, -1)$ again reduces the peak sound pressure level by about 5dB, but produces a much larger reduction than the previous (supersonic) case at large upstream angles.

# 6 Conclusions and future work

It was shown that the high-frequency Lilley's-equation solution developed in Ref. [3] for a doubly-infinite, transversely-sheared mean flow also applies to the noise generated internally within a nozzle, provided appropriate boundary conditions are imposed on the ray trajectories at the surface of the duct and a suitable wall impedance factor is included.

By assuming the turbulence to be axisymmetric about the mean flow di-

rection, a simplified expression for the far-field sound radiated by a turbulent flow within the nozzle was derived.

The analysis was applied to the case of a round duct with an axisymmetric mean flow, and it was shown that a hard-walled duct has no effect on the far-field sound radiated at polar angles sufficiently close the duct axis (but outside the zone of silence). The numerical results show that the duct cuts off some of the rays for polar angles in the upstream quadrant, and that acoustic liners can significantly reduce the far-field sound but their effectiveness depends upon the wall impedance, source position and mean flow field. The analysis can be used to carry out detailed parametric studies to find the optimal wall impedance, acoustic source distributions, mean profile shape and nozzle geometry for a given application.

The ray acoustics solution has the advantage of being applicable to nozzles of any shape and any mean velocity profile (see Fig. 1). The high-speed civil transport was expected to use a rectangular mixer-ejector nozzle with a very complex mean velocity profile and acoustically treated walls. Future work will evaluate the ray acoustics solution for this geometry and make comparisons with some recent test data.

This paper only considers the sound produced by the first source term in

Eq. (4) - the so-called 'self-noise' term. While this term is asymptotically large compared with the second (or 'shear-noise') term in Eq. (4) in the high- frequency limit, it may be necessary to include the latter in order to obtain agreement with experimental results, particularly in the downstream quadrant (see, for example, Khavaran [14]).

This paper also does not address the diffracted radiation produced by acoustic rays striking the duct lip. It too is asymptotically small compared with the direct and reflected sound (Pierce [7]), but can still be of significance at the upstream polar angles, where most of the direct or reflected sound is cut off by the duct. This is currently being investigated by Wundrow and Goldstein [15], who plan to develop a computational algorithm incorporating the diffraction effects into the present analysis.

The authors would like to thank Dr. James Bridges of NASA Glenn Research Center for providing values of the wall impedance and Dr. Abbas Khavaran of Dynacs Engineering Co. for information on the mixer-ejector nozzle configuration and flow field.

# References


[1] Goldstein, M.E., and Rosenbaum, B. M., "Emission of Sound from Turbulence Convected by a Parallel Flow in the Presence of Solid Boundaries," NASA TN D-7118, Feb 1973.

[2] Dill, L. H., Oyediran, A. A., and Krejsa, E. A., "Refraction of Sound Emitted Near Solid Boundaries From a Sheared Jet,"NASA TM 1998-207421, May 1998.

[3] Goldstein, M.E., "High Frequency Sound Emission From Moving Point Multipole Sources Embedded in Arbitrary Transversely Sheared Mean Flows," *J. Sound and Vib.*, Vol. 80, No. 4, pp. 499-522.

[4] Durbin, P. A., "High Frequency Green Function for Aerodynamic Noise in Moving Media, Part I: General Theory,"*J. Sound and Vib.*, Vol. p1, No. 4, pp. 519-525.

[5] Durbin, P. A., "High Frequency Green Function for Aerodynamic Noise in Moving Media, Part II: Noise From a Spreading Jet,"*J. Sound and Vib.*, Vol. p1, No. 4, pp. 527-538.

[6] Goldstein, M. E., *Aeroacoustics*, McGraw-Hill, 1976, pp. 249 - 259.

[7] Pierce, A.D., *Acoustics: An Introduction to Its Physical Principles and Applications*, McGraw-Hill, 1981, pp. 107 - 110, and 479 - 494.

[8] Boyd, W. K., Kempton, A.J. and Morfey, C.L., "Ray-Theory Predictions of the Noise Radiated from Aeroengine Ducts," AIAA paper 84-2332, 1984.

[9] Millionschikov, M. D., "Theory of Homogeneous Isotropic Turbulence," *Dokl. Akad. Nauk. SSR*, Vol. 32, no. 9, pp.611-614.

[10] Batchelor, G.K., *Theory of Homogeneous Turbulence*, Cambridge University Press, 1960, p. 179.

[11] Goldstein, M.E., and Rosenbaum, B. M., "Effect of Anisotropic Turbulence on Aerodynamic Noise," *J. Acous. Soc. Am.*, Vol. 54, No. 3, 1973. pp. 630-645.

[12] Kerschen, E. J., "Constraints on the Invariant Functions of Axisymmetric Turbulence," *AIAA J.* , Vol. 21, No. 7, 1983, pp. 978-985.

[13] Béchara, W., Lafon, P., Bailly, C, and Candel, S.M., "Application of a $\kappa - \epsilon$ Turbulence Model to the Prediction of Noise for Simple

and Coaxial Free Jets," *J. Acous. Soc. Am.*, Vol. 97, No. 6, 1995, pp. 3518-3531.

[14] Khavaran, A., "On the Role of Anisotropy in Turbulent Mixing Noise," Submitted to *AIAA J.*

[15] Wundrow, D.W. and Goldstein, M.E., "Diffraction of High-Frequency Sound Convected by a Parallel Mean Flow Through a Semi-Infinite Duct," In preparation.

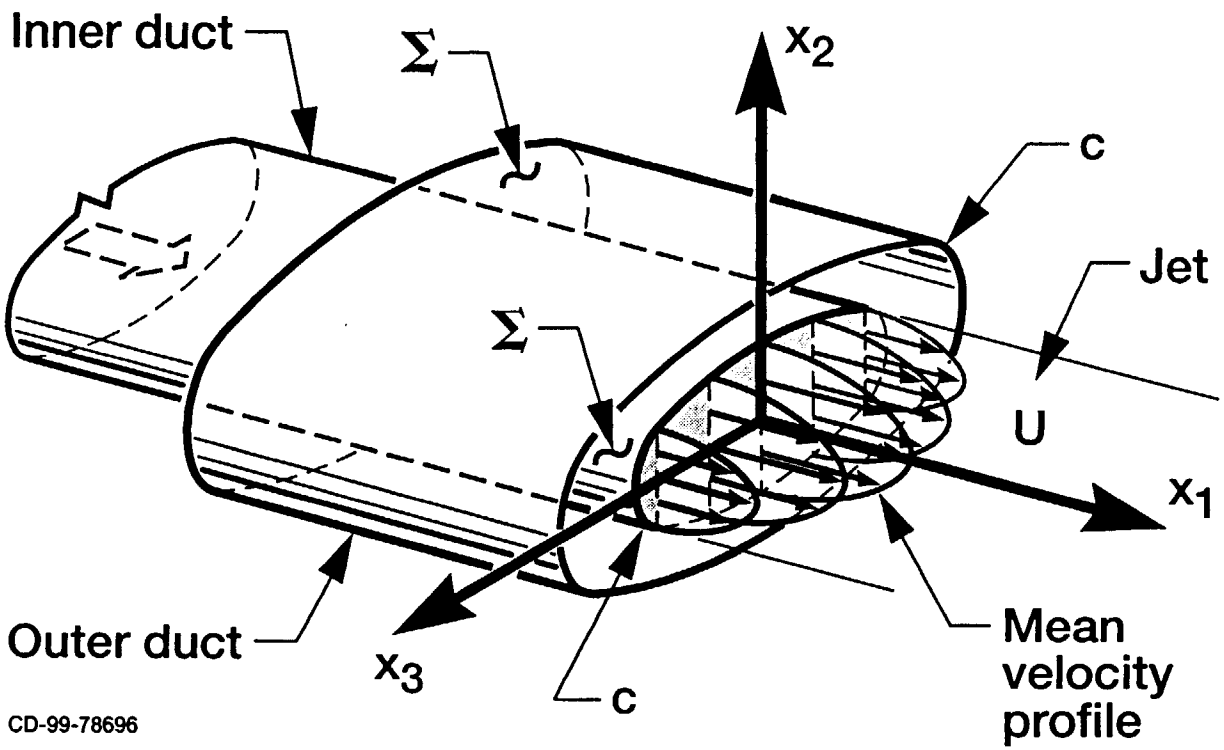


Fig 1-b Example of more complex configuration to which analysis applies

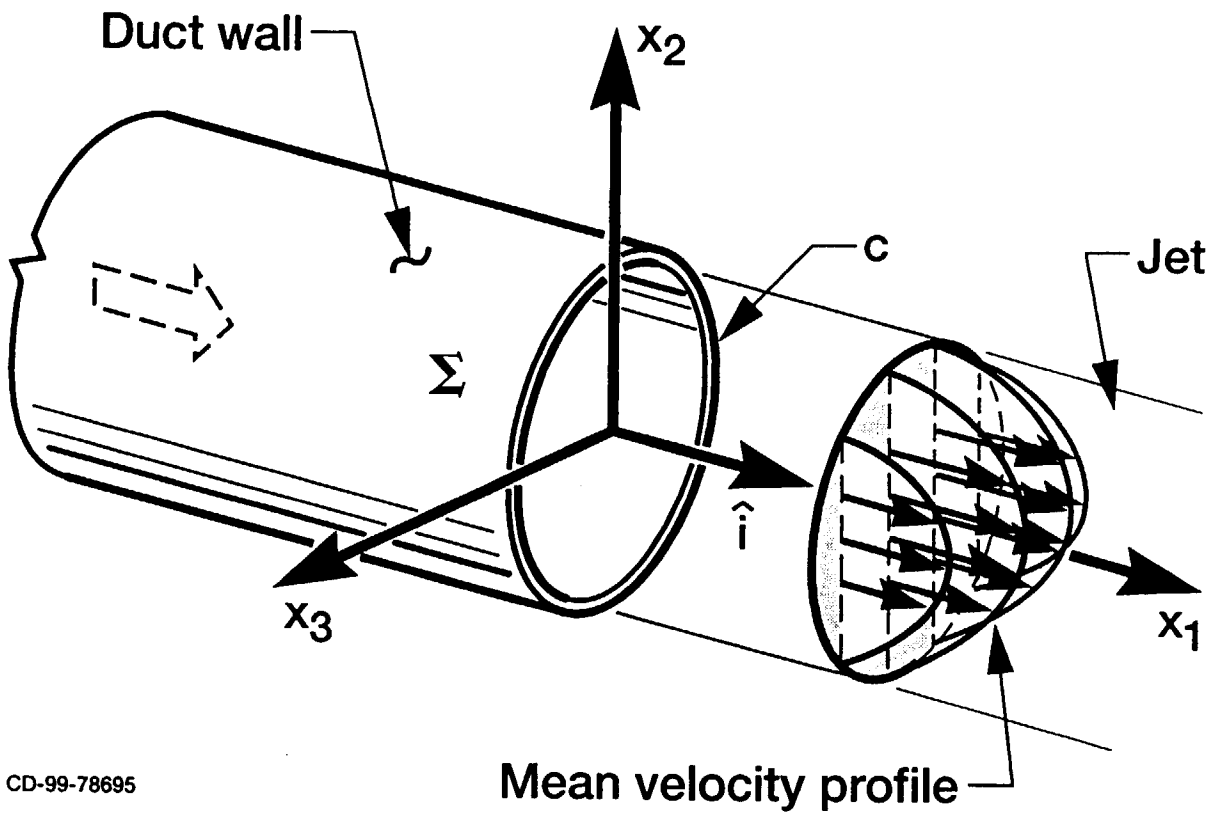


Fig 1-a Flow configuration

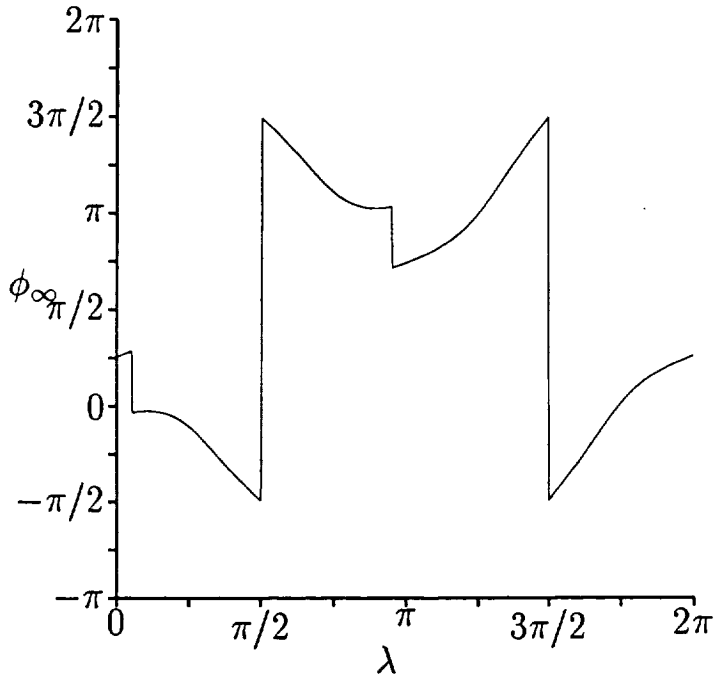


Figure 2: Far-field cirumferential angle vs. initial cirumferential angle for Mach number profile (70) with $a = 0.1, b = 6, M(0) = 0.9$ and source position $r_s = 0.75r_0, x_1{}^s = -0.5r_0$, and $\theta_\infty = 3\pi/8$.

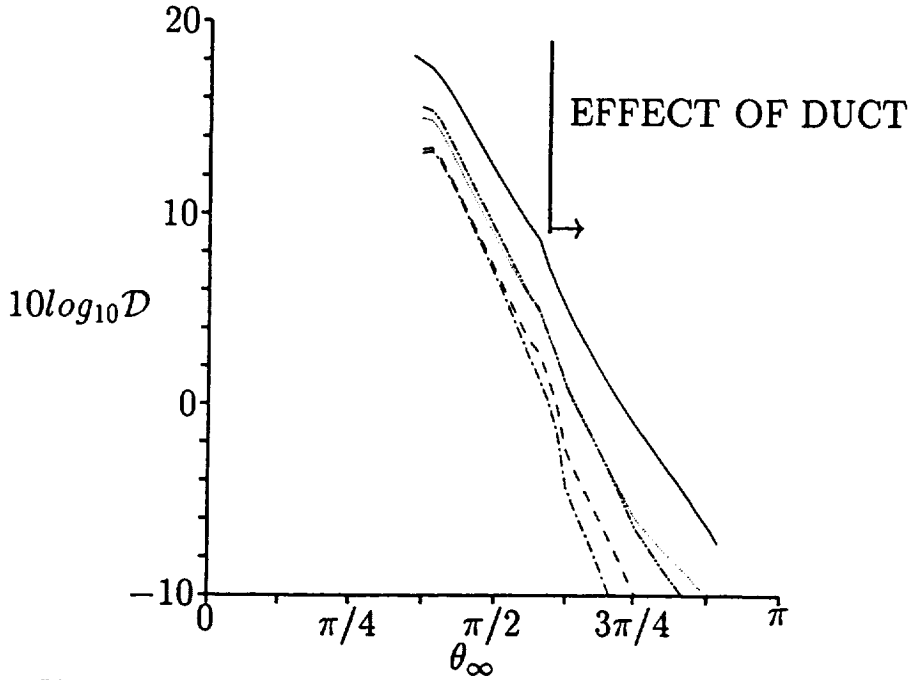


Figure 3: Far-field spectral directivity for Mach number profile (70) with $a = 0.1, b = 6, M(0) = 1.5$, and source position $r_s = 0.75r_0, x_1^s = -2.0r_0$ for hard-wall duct (solid) and soft-wall duct with $\zeta = (1, -1)$ (dashed), $(1/2, -1)$ (dotted), $(2, -1)$ (dot-dashed), $(1, -2)$ (dot-dot-dashed).

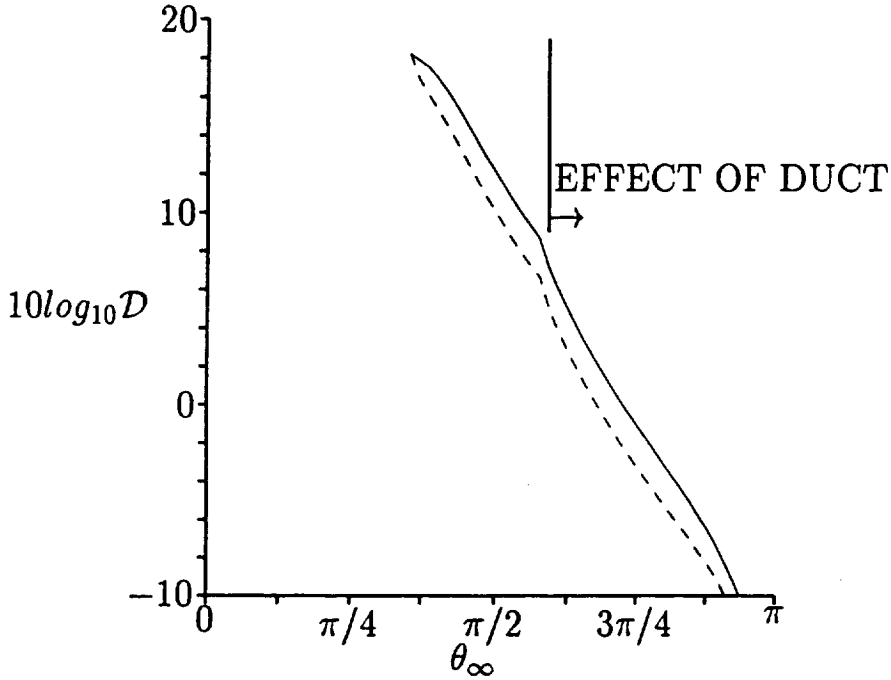


Figure 4: Far-field spectral directivity for Mach number profile (70) with $a = 0.1, b = 6, M(0) = 1.5$, and source position $r_s = 0.75r_0, x_1{}^s = -0.5r_0$ for hard-wall duct (solid) and soft-wall duct with $\zeta = (1, -1)$ (dashed).

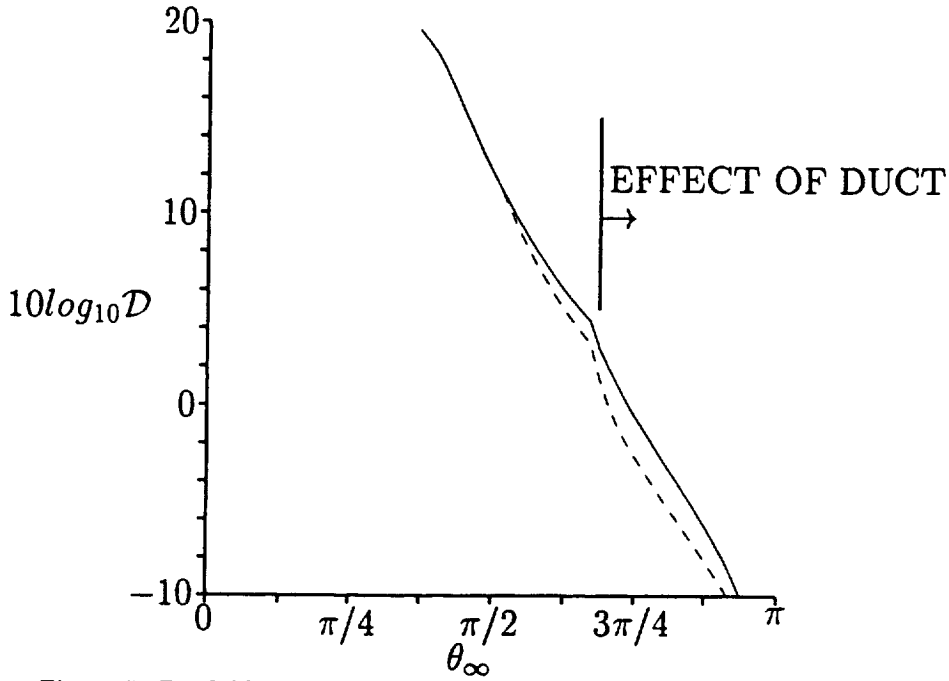


Figure 5: Far-field spectral directivity for Mach number profile (70) with $a = 0.1, b = 6, M(0) = 1.5$, and source position $r_s = 0.5r_0, x_1^s = -0.5r_0$ for hard-wall duct (solid) and soft-wall duct with $\zeta = (1, -1)$ (dashed).

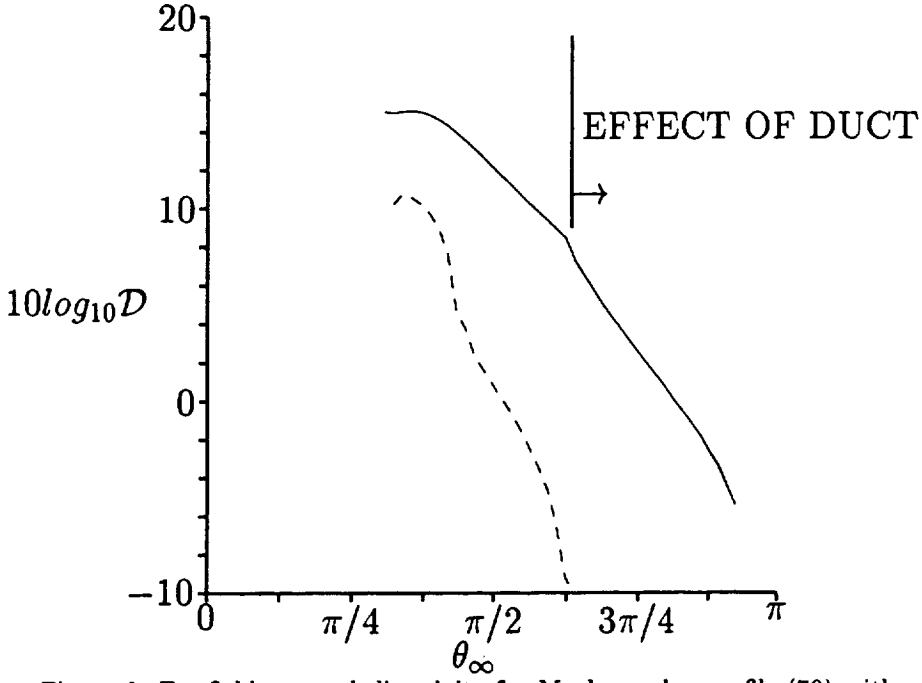


Figure 6: Far-field spectral directivity for Mach number profile (70) with $a = 0.1, b = 6, M(0) = 0.9$, and source position $r_s = 0.5r_0, x_1^s = -2.0r_0$ for hard-wall duct (solid) and soft-wall duct with $\zeta = (1, -1)$ (dashed).

# List of Figure Captions

Figure - 1 (a)Flow configuration. (b) Example of more complex configuration to which analysis applies.

Figure - 2 Far-field cirumferential angle vs. initial cirumferential angle for Mach number profile (70) with $a = 0.1, b = 6, M(0) = 0.9$ and source position $r_s = 0.75r_0, {x_1}^s = -0.5r_0$, and $\theta_\infty = 3\pi/8$.

Figure - 3 Far-field spectral directivity for Mach number profile (70) with $a = 0.1, b = 6, M(0) = 1.5$, and source position $r_s = 0.75r_0, {x_1}^s = -2.0r_0$ for hard-wall duct (solid) and soft-wall duct with $\zeta = (1, -1)$ (dashed), $(1/2, -1)$ (dotted), $(2, -1)$ (dot-dashed), $(1, -2)$ (dot-dot-dashed).

Figure - 4 Far-field spectral directivity for Mach number profile (70) with $a = 0.1, b = 6, M(0) = 1.5$, and source position $r_s = 0.75r_0, {x_1}^s = -0.5r_0$ for hard-wall duct (solid) and soft-wall duct with $\zeta = (1, -1)$ (dashed).

Figure - 5 Far-field spectral directivity for Mach number profile (70) with $a = 0.1, b = 6, M(0) = 1.5$, and source position $r_s = 0.5r_0, {x_1}^s = -0.5r_0$ for hard-wall duct (solid) and soft-wall duct with $\zeta = (1, -1)$ (dashed).

Figure - 6 Far-field spectral directivity for Mach number profile (70) with $a = 0.1, b = 6, M(0) = 0.9$, and source position $r_s = 0.5r_0, {x_1}^s = -2.0r_0$ for hard-wall duct (solid) and soft-wall duct with $\zeta = (1, -1)$ (dashed).